2019 57th Annual Allerton Conference on Communication, Control, and Computing
(Allerton)
Allerton Park and Retreat Center
Monticello, IL, USA, September 24-27, 2019

Optimal Grid – Distributed Energy Resource Coordination: Distribution Locational Marginal Costs and Hierarchical Decomposition

Panagiotis Andrianesis[1] and Michael C. Caramanis[2]

Abstract— **We consider radial distribution networks hosting Distributed Energy Resources (DERs), including Solar Photovoltaic (PV) and storage-like loads, such as Electric Vehicles (EVs). We employ short-run dynamic Distribution Locational Marginal Costs (DLMCs) of real and reactive power to co-optimize distribution network and DER schedules. Striking a balance between centralized control and distributed self-dispatch, we present a novel hierarchical decomposition approach that is based on centralized AC Optimal Power Flow (OPF) interacting with DER self-dispatch that adapts to real and reactive power DLMCs. The proposed approach is designed to be highly scalable for massive DER Grid integration with high model fidelity incorporating rigorous network component dynamics and costs and reflecting them in DLMCs. We illustrate the use of an Enhanced AC OPF to discover spatiotemporally varying DLMCs enabling optimal Grid-DER coordination incorporating congestion and asset (transformer) degradation. We employ an actual distribution feeder to exemplify the use of DLMCs as financial incentives conveying sufficient information to optimize Distribution Network and DER (PV and EV) operation, and we discuss the applicability and tractability of the proposed approach, while modeling the full complexity of spatiotemporal DER capabilities and preferences.**

I. Introduction

With Distributed Energy Resources (DERs), including Solar Photovoltaic (PV) and storage-like loads such as Electric Vehicles (EVs) with Volt/VAR capabilities, emerging as a major user of distribution grid infrastructure, the grid is becoming increasingly active, distributed, dynamic, and challenging to plan and operate [1]. As such, DERs are bound to have a profound impact on the adequacy of T&D assets, efficient grid operation, reliability, and security of supply, and hence their scheduling will be crucial. We argue that optimal DER scheduling depends on dynamic Distribution Locational Marginal Costs (DLMCs) [2], [3], [4], [5], [6], whose accurate estimation is expected to bring about fundamental changes in distribution planning, operation, and eventually power markets.

Unsurprisingly, DER scheduling and coordination with the grid and its assets in the context of distribution network operational planning is attracting increasing attention. Emerging literature focuses on the extension of wholesale Locational Marginal Price (LMP) markets to the distribution network through reliance on Distribution LMPs (DLMPs) [2], [3], [4], [7], [8], [9]. A variety of suggested approaches and models have attempted to do just that by considering uniform price-quantity bidding DERs and/or using DC Optimal Power Flow (OPF) models. However, we argue that existing transmission market-clearing approaches do not extend to Distribution Networks. Current wholesale markets determine spatiotemporal, i.e., location and time specific, marginal cost-based prices [10], [11], clear over large energy balancing areas, and for all intents and purposes they manage nodal market participant uniform price-quantity bids, which, under competitive conditions, represent the short-run marginal cost (for generators) or marginal utility (for wholesalers). Such markets have resulted in significant operational efficiency improvements and have provided participants with strong incentives to improve their actual costs through better maintenance and innovation adoption. However, small DER prosumers connected at the low voltage distribution network have been so far left out of dynamic short-run marginal cost based markets, facing instead average cost volumetric rates. Contrary to the transmission system where centralized generation is scheduled through linear DC OPF models, optimal distribution-grid connected DER scheduling requires AC OPF formulations (see e.g., [2], [9] that employ the *branch flow* (a.k.a. DistFlow) equations, introduced for radial networks by [12], and in fact their relaxation to convex Second Order Cone constraints proposed by [13]), to accurately calculate real/reactive power flows, and ensure the engineering (current and voltage) limits are respected. A comprehensive analysis of several approaches in decomposing and interpreting real and reactive power DLMPs in the AC OPF context is provided in [14]. In [2], DLMPs are extended to include reserves — apart from real/reactive power — and an iterative distributed architecture is sketched capturing DER intertemporal preferences and physical system dynamics.

Apart from nodal voltage congestion, sustained transformer overloading in distribution networks also renders the explicit modeling of reactive power a *must* in the context of a 24-hour ahead AC OPF capable of modeling Volt/VAR control, ampacity constrained feeders, intertemporally coupled transformer life degradation and complex DER/EV charging preferences. Interestingly, early studies on EVs [15] pointed out that the clustering of EV chargers under the same transformer may cause damage and outages from persistent overloading. More recently, a study on the Sacramento Municipal Utility District [16] estimated that a high PV penetration would cause overvoltages (by at least 5% of nominal) to about 26% of the substations and service transformers, and that a high EV penetration would

* This work was partially supported by the Sloan Foundation under grant G-2017-9723 and NSF AitF grant 1733827.

[1] Panagiotis Andrianesis is with the Division of Systems Engineering, Boston University, Boston, MA panosa@bu.edu

[2] Michael C. Caramanis is with the Department of Mechanical Engineering and the Division of Systems Engineering, Boston University, Boston, MA mcaraman@bu.edu

cause overloads to up to 17% of the approximately 12,000 service transformers (exceeding 140% the nameplate rating) with an average estimated cost of $7,400 per transformer replacement. Notably, the 2017 FERC Financial Form I filing by Commonwealth Edison, a typical urban distribution Utility, reports the original cost of line transformers at 8% of the total cost of the Electric Plant. Indeed, several works study the impact of EVs on distribution transformers [17], [18], [19], [20], [21], and the acceleration of transformer degradation from increasing EV penetration, noting that transformer aging is dependent upon the thermal effects of persistent transformer loading. Furthermore, it is shown that rooftop solar may utilize their inverters by adjusting their power factor to mitigate overvoltages, and that the transformer thermal time constant may allow PV generation to reduce the transformer temperature when EVs are charging [22], with a beneficial impact on transformer Loss of Life (LoL).[1] However, these simulation studies do not internalize transformer degradation to the operational planning problem.

In this paper, we employ short-run dynamic DLMCs of real and reactive power to co-optimize distribution network and DER schedules. Striking a balance between centralized control and distributed self-dispatch, we present a novel hierarchical decomposition approach that is based on centralized AC OPF capability interacting with DER self-dispatch that adapts to real and reactive power DLMCs. The proposed approach is designed to be highly scalable allowing for massive DER participation with high model fidelity that captures precise estimation and cost inclusiveness of DLMCs. We illustrate that the discovery of spatiotemporally varying DLMCs, using an enhanced AC OPF model, which apart from network congestion also reflects transformer degradation, is key to optimal Grid - DER coordination. We employ actual distribution feeders to exemplify the use of DLMCs as financial incentives that convey sufficient information to optimize Distribution Network, and DER (PV and EV) operation, and we discuss the applicability and tractability of the proposed approach, while modeling the full complexity of spatiotemporal DER capabilities and preferences.

The remainder of the paper is organized as follows. In Section II, we present the distributed self-dispatch DER models, and in Section III, we present the formulation of a centralized, enhanced AC OPF model. In Section IV, we discuss the implications of the optimal Grid - DER coordination, in the context of the operational planning problem. In Section V, we highlight the ideas of a hierarchical decomposition approach, and in Section VI we illustrate its applicability on an actual distribution feeder. Lastly, in Section VII, we conclude and provide directions for further research.

[1]The life of a distribution transformer is estimated at about 20 years (180,000 hours), assuming operation at a reference Hottest Spot Temperature (HST) of 110^oC (insulation designed for an average winding temperature of 65^oC). IEEE Standard C.57.91-2011 [23] and IEC Standard 60076-7:2018 [24] provide guidelines for transformer loading and propose an exponential representation of the aging acceleration factor in terms of the HST when it exceeds 110^oC. In particular, for HSTs exceeding (being lower than) 110^oC, the aging acceleration factor is greater (less) than 1.

II. DER Models

In this section, we present DER self-dispatch models, for solar PVs (in Subsection II-A) and EVs (in Subsection II-B), in the context of a general multi-period (day-ahead) problem setting, accommodating smart inverter capabilities and EV mobility (EVs can be connected at different nodes during the time horizon).

A. PV Model

Let us consider a self-scheduling rooftop solar PV s, which is offered a price $\hat{\lambda}^P_t$ for the provision of real power at time period t, denoted by $p_{s,t}$, and a price $\hat{\lambda}^Q_t$ for the provision of reactive power, denoted by $q_{s,t}$. PV s can use its smart inverter capabilities and adjust its power factor, aiming at maximizing its revenues from the provision of real and reactive power over the optimization horizon, as follows:

$$\max_{p_{s,t},q_{s,t}} \sum_t \hat{\lambda}^P_t p_{s,t} + \sum_t \hat{\lambda}^Q_t q_{s,t}. \tag{1}$$

PV constraints are as follows:

$$p_{s,t} \leq \tilde{C}_{s,t}, \quad \forall s,t \in \mathcal{T}_I, \tag{2}$$

$$p^2_{s,t} + q^2_{s,t} \leq C^2_s, \quad \forall s,t \in \mathcal{T}_I, \tag{3}$$

$$p_{s,t} = q_{s,t} = 0, \qquad \forall s,t \notin \mathcal{T}_I, \tag{4}$$

with $p_{s,t} \geq 0$, and $\mathcal{T}_I \subset \mathcal{T}^+$ the subset of time periods for which $\rho_t > 0$. Constraints (2) impose limits on the real power, based on the adjusted PV nameplate capacity, $\tilde{C}_{s,t} = \rho_t C_s$, where $\rho_t \in [0,1]$ is the irradiation level, and C_s the nameplate capacity. Constraints (3) impose limits on real and apparent power assuming an appropriately sized inverter, whereas constraints (4) impose zero generation when $\rho_t = 0$. We note that this model does not account for using the smart inverter at night, but an extension to include such a capability is straightforward.

Hence, the following optimization problem, referred to as **PV-opt**, describes a self-scheduling PV that adapts its real/reactive power profile to the offered real and reactive power prices.

$$\textbf{PV-opt:} \quad (1) \quad \textit{subject to:} \quad (2)-(4). \tag{5}$$

We note that PV-opt can be solved in parallel for each time period, since there are no intertemporal constraints. Evidently, if $\hat{\lambda}^P_t$ is negative, then PV s will select to produce no real power, setting $p_{s,t} = 0$. If $\hat{\lambda}^Q_t$ is positive (negative), then PV s will adjust its power factor to provide (consume) reactive power, i.e., $q_{s,t} > 0$ ($q_{s,t} < 0$), so that the term $\hat{\lambda}^Q_t q_{s,t}$ is positive.

B. EV Model

Let us consider a self-scheduling EV e, which is offered a price $\hat{\lambda}^P_t$ for consuming real power at time period t, denoted by $p_{e,t}$, and a price $\hat{\lambda}^Q_t$ for consuming reactive power, $q_{s,t}$, at the node that it is connected during each time period. EV

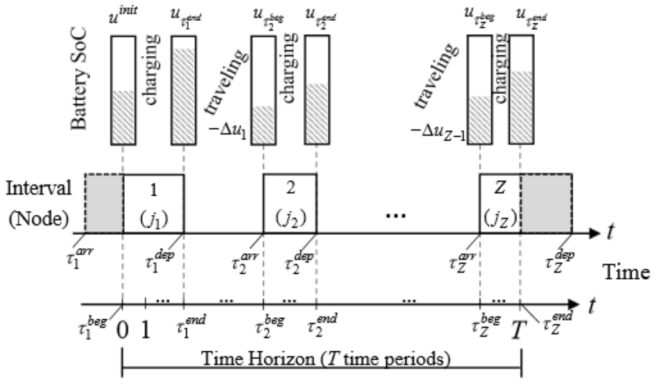

Fig. 1. General case of EV charging intervals during the optimization time horizon, with first interval beginning in the previous day ($\tau_1^{beg} = 0$), and last interval ending in the following day ($\tau_Z^{end} = T$).

e employs its EV charger so as to minimize its net charging cost over the daily cycle:

$$\min_{p_{e,t},q_{e,t}} \sum_t \hat{\lambda}_t^P p_{e,t} + \sum_t \hat{\lambda}_t^Q q_{e,t}, \tag{6}$$

Assume an EV that is connected for Z intervals, at nodes $j_1, ..., j_Z$. Let τ_z^{arr} (τ_z^{dep}), for $z = 1, ..., Z$, denote the periods at which an arrival (departure) occurs. In general, as illustrated in Fig. 1, intervals 1 (first) and Z (last) may not entirely fit within the time horizon. Hence, let $\mathcal{T}^{beg} = \{\tau_z^{beg}\}$ and $\mathcal{T}^{end} = \{\tau_z^{end}\}$ be the sets of time periods of interval z, for $z = 1, ..., Z$, denoting an adjusted beginning and end, respectively, considering only the part of the interval within the time horizon. Also, let $\mathcal{T}_z = \{\tau_z^{beg} + 1, ..., \tau_z^{end}\}$ be the set of time periods of interval z, for $z = 1, .., Z$, during which the EV is connected at node j_z. In what follows, we add in the aforementioned sets the EV subscript e, which was omitted for simplicity.

The State of Charge (SoC) of EV e is described by variable $u_{e,t}$ for time periods $t \in \mathcal{T}_e^{beg} \cup \mathcal{T}_e^{end}$. The SoC is reduced by $\Delta u_{z,e}$ after departure z and until arrival $z+1$, for $z = 1, .., Z_e - 1$. EV constraints are as follows:

$$u_{e,\tau_1^{beg}} = u_e^{init}, \quad \forall e, \tag{7}$$

$$u_{e,\tau_z^{end}} = u_{e,\tau_z^{beg}} + \sum_{t \in \mathcal{T}_{e,z}} p_{e,t}, \quad \forall e, z = 1, ..., Z_e, \tag{8}$$

$$u_{e,\tau_{z+1}^{beg}} = u_{e,\tau_z^{end}} - \Delta u_{e,z}, \quad \forall e, z = 1, ..., Z_e - 1, \tag{9}$$

$$u_{e,t}^{min} \leq u_{e,t} \leq C_e^B, \quad \forall e, t \in \mathcal{T}_e^{end}, \tag{10}$$

$$0 \leq p_{e,t} \leq C_r, \quad \forall e, t \in \cup_{z=1}^{Z_e} \mathcal{T}_{e,z}, \tag{11}$$

$$p_{e,t}^2 + q_{e,t}^2 \leq C_e^2, \quad \forall e, t \in \cup_{z=1}^{Z_e} \mathcal{T}_{e,z}, \tag{12}$$

$$p_{e,t} = q_{e,t} = 0, \quad \forall e, t \in \mathcal{T}^+ \setminus \cup_{z=1}^{Z_e} \mathcal{T}_{e,z}, \tag{13}$$

with $p_{e,t}, u_{e,t} \geq 0$. Eq. (7) initializes the SoC (u_e^{init}) at τ_1^{beg}, (8) and (9) define the SoC at the end/beginning of an interval, after charging/traveling, respectively. Constraints (10) impose a minimum SoC, $u_{e,t}^{min}$, at the end of an interval as well as the limit of the EV battery capacity, C_e^B. Constraints (11) impose the limit of the charging rate, C_r, which is related to the capacity of the EV battery charger, whereas constraints (12) impose the limits of the charge, C_e, which is related to the size of the inverter. Lastly, (13) imposes zero consumption when the EV is not plugged in.

Hence, the following optimization problem, referred to as **EV-opt**, describes a self-scheduling EV that adapts its real/reactive power charging profile to the offered real and reactive power prices.

$$\textbf{EV-opt:} \quad (6) \quad \textit{subject to:} \quad (7) - (13). \tag{14}$$

Unlike PV-opt, EV-opt includes intertemporal constraints, and, hence, it cannot be solved in parallel. Evidently, if $\hat{\lambda}_t^Q$ is positive (negative), then the EV will provide (consume) reactive power, i.e., $q_{e,t}$ will be negative (positive), so that the term $\hat{\lambda}_t^Q q_{e,t}$ is negative thus reducing the charging cost.

III. Distribution Network AC OPF Model

We consider a radial network with $N+1$ nodes and N lines. Let $\mathcal{N} = \{0, 1, ..., N\}$ be the set of nodes, with node 0 representing the root node, and $\mathcal{N}^+ \equiv \mathcal{N} \setminus \{0\}$. Let $\mathcal{L}$ be the set of lines, with each line denoted by the pair of nodes (i, j) it connects — henceforth ij for short, where node i refers to the (unique due to the radial structure) preceding node of $j \in \mathcal{N}^+$. Transformers are represented as a subset of lines, denoted by $y \in \mathcal{Y} \subset \mathcal{L}$. For node $i \in \mathcal{N}$, v_i denotes the magnitude squared voltage. For node $j \in \mathcal{N}^+$, p_j and q_j denote the net demand of real and reactive power, respectively. A positive (negative) value of p_j refers to withdrawal (injection); similarly for q_i. Net injections at the root node are denoted by P_0 and Q_0, for real and reactive power, respectively. These are positive (negative) when power is flowing from (to) the transmission system. For each line ij, with resistance r_{ij} and reactance x_{ij}, l_{ij} denotes the magnitude squared current, P_{ij} and Q_{ij} the sending-end real and reactive power flow, respectively.

For the purposes of this section, we assume that the real and reactive power net injections at each node are known (fixed). In such case, the main decision variable is the voltage of the substation; once this is decided, then the model practically reduces to a load flow model.

The centralized AC OPF problem aims at minimizing the aggregate real and reactive power cost and the transformer degradation cost, as follows:

$$\min \overbrace{\sum_t c_t^P P_{0,t}}^{\text{Real Power Cost}} + \overbrace{\sum_t c_t^Q Q_{0,t}}^{\text{Reactive Power Cost}} + \overbrace{\sum_{y,t} c_y f_{y,t}}^{\text{Transformer Cost}}, \tag{15}$$

where c_t^P is the real power cost — typically the LMP at the T&D interface (substation), c_t^Q is the opportunity cost for the provision of reactive power, c_y is an hourly transformer cost representing the cost for losing one hour of life, and $f_{y,t}$ is the transformer aging acceleration factor. Hence the last term in (15) represents the aggregate cost of the transformers' LoL resulting from their loading conditions in the optimization horizon.

The constraints of the AC OPF problem are based on the relaxed *branch flow* model, supplemented by voltage and ampacity limits and transformer-related constraints. In what follows, and unless otherwise mentioned, $j \in \mathcal{N}^+$, and $t \in \mathcal{T}^+$, with $\mathcal{T} = \{0, 1, ..., T\}$, $\mathcal{T}^+ \equiv \mathcal{T} \setminus \{0\}$, and T the length of the optimization horizon.

$$P_{0,t} = P_{01,t} \rightarrow (\lambda^P_{0,t}), \quad \forall t, \tag{16}$$

$$Q_{0,t} = Q_{01,t} \rightarrow (\lambda^Q_{0,t}), \quad \forall t, \tag{17}$$

$$P_{ij,t} - r_{ij} l_{ij,t} = \sum_{k:j\rightarrow k} P_{jk,t} + p_{j,t} \rightarrow (\lambda^P_{j,t}), \quad \forall j, t, \tag{18}$$

$$Q_{ij,t} - x_{ij} l_{ij,t} = \sum_{k:j\rightarrow k} Q_{jk,t} + q_{j,t} \rightarrow (\lambda^Q_{j,t}), \quad \forall j, t, \tag{19}$$

$$v_{j,t} = v_{i,t} - 2r_{ij}P_{ij,t} - 2x_{ij}Q_{ij,t}) + \left(r^2_{ij} + x^2_{ij}\right) l_{ij,t}, \quad \forall j, t, \tag{20}$$

$$v_{i,t} l_{ij,t} \geq P^2_{ij,t} + Q^2_{ij,t} \quad \forall j, t. \tag{21}$$

$$\underline{v}_i \leq v_{i,t} \leq \bar{v}_i \rightarrow (\underline{\mu}_{i,t}, \bar{\mu}_{i,t}), \quad \forall i, t, \tag{22}$$

$$l_{ij,t} \leq \bar{l}_{ij} \rightarrow (\bar{\nu}_{j,t}), \quad \forall j, t, \tag{23}$$

$$f_{y,t} \geq \alpha_\kappa h_{y,t} + \beta_{y,\kappa} l_{y,t} + \gamma_{y,\kappa} \rightarrow (\xi_{y,t,\kappa}), \forall y, t, \kappa, \tag{24}$$

$$h_{y,t} = \delta h_{y,t-1} + \epsilon_y l_{y,t} + \zeta_{y,t}, \quad \forall y, t. \tag{25}$$

Constraints (16)–(19) define the real and reactive power balance. Constraint (20) defines the voltage drop along a line. Inequality (21) is the Second Order Cone Programming (SOCP) relaxation — introduced by [13] — of the (non-convex) equality constraint that defines apparent power. Constraints (22) and (23) represent voltage limits and ampacity limits, where $\underline{v}_i$, $\bar{v}_i$, and $\bar{l}_{ij}$ are the lower voltage, upper voltage, and line ampacity limits (squared), respectively. Constraints (24) represent a piecewise linearization of the exponential aging acceleration factor — note that $f_{y,t} \geq 0$, with $\kappa = 1, ..., M$, where M is the number of segments — see [5, Fig. 1] for a graphical illustration, and $h_{y,t}$ the transformer top-oil temperature. The coefficients α_κ, $\beta_{y,\kappa}$, and $\gamma_{y,\kappa}$ are transformer specific, and they are related to the slope of the aging acceleration factor *w.r.t.* the transformer HST, and the transformer winding thermal response. Their detailed formulas and recommended values are found in [5]. Constraints (25) are a linear recursive equation that defines the transformer top-oil temperature. Coefficient δ plays an important role in the intertemporal impact of the transformer degradation cost; its value — always less than 1 — depends on the time granularity of the problem. Using the recommended distribution transformer constants, for time periods equal to 1 hour, 30 minutes or 15 minutes, δ will be 0.75, 0.857 or 0.923, respectively. The coefficients ϵ_y, and $\zeta_{y,t}$ are transformer specific, related to the top-oil thermal response, and the latter one also depends on the ambient temperature. Their detailed formulas and recommended values are found in [5]. Dual variables of constraints (16)–(19), (22), (23), and (24) are shown in parentheses.

The resulting relaxed AC OPF problem is a convex SOCP problem — referred to as **Net-opt** — and is summarized as follows:

$$\textbf{Net-opt:} \quad (15) \quad \textit{subject to:} \quad (16) - (25). \tag{26}$$

We note the following interesting remarks. First, we refer the interested reader to recent works that discuss and propose remedies for cases when the relaxation presented in (21) — which defines the apparent power but can also be viewed as a definition of the current — is not exact [25], [26], [27], [28], [29]. We note that we did not encounter such cases in our numerical illustration. Second, the linear inequality constraints (24) that define the aging acceleration factor $f_{y,t}$ are also a relaxation of the piecewise linear representation, which would otherwise require the introduction of binary variables. However, since $c_y > 0$, it is straightforward to show that at least one of the above inequalities should be binding (at equality), and hence this relaxation is exact. In fact, since $f_{y,t}$ is actually related to the line current values, $l_{y,t}$, we expect that the transformer degradation costs would mitigate the results obtained in cases when the relaxation in (21) is not exact. Third, it is important to note that the transformer model thermal response is very accurately represented in our optimization problem mainly due to: (i) the fact that the dynamics of the thermal response fit nicely the time granularity of the operational planning problem, since the top-oil thermal time constant (of about 3 hours) allows us to consider difference equations whereas the winding thermal time constant (of about 4 minutes) allows us to consider a steady state, and (ii) the fact that the branch flow variable $l_{y,t}$, which represents the magnitude squared of the current, allows us to define the square of the ratio of the transformer load to the rated load using a linear equation, hence fitting nicely the thermal response to the branch flow model. Lastly, we note that the intertemporal impact in the transformer degradation cost that extends beyond the optimization horizon — typical to many scheduling problems — can be captured by rolling horizon approaches or by requiring the transformer temperature at the end of the horizon to less than or equal to a certain target value (e.g., the value at the beginning of the horizon).

IV. Optimal Grid - DER Coordination

In the previous sections, we presented the two basic optimization modules related to DERs and distribution networks separately. In this section, we present the links between the two modules.

First, the two modules are linked through the net demand at each node. More specifically, the real power net demand $p_{j,t}$ includes the aggregate effect of conventional loads, EVs, and PVs, denoted by sets $\mathcal{D}$, $\mathcal{E}$, and $\mathcal{S}$, as follows:

- Conventional demand consumption $p_{d,t}$ of load $d \in \mathcal{D}_j$, where $\mathcal{D}_j \subset \mathcal{D}$ is the subset of loads connected at node j;
- consumption $p_{e,t}$ of EV $e \in \mathcal{E}_{j,t}$, where $\mathcal{E}_{j,t} \subset \mathcal{E}$ is the subset of EVs that are connected at node j, during time period t, and

- Generation $p_{s,t}$ of PV (rooftop solar) $s \in \mathcal{S}_j$, where $\mathcal{S}_j \subset \mathcal{S}$ is the subset of PVs connected at node j.

Similarly for reactive power net demand $q_{j,t}$, and the conventional demand consumption $q_{d,t}$ of load d, consumption $q_{e,t}$ of EV e, and generation $q_{s,t}$ of PV s. For clarity, the definitions of aggregate dependent variables are listed below:

$$p_{j,t} = \sum_{d \in \mathcal{D}_j} p_{d,t} + \sum_{e \in \mathcal{E}_{j,t}} p_{e,t} - \sum_{s \in \mathcal{S}_j} p_{s,t}, \quad \forall j, t, \tag{27}$$

$$q_{j,t} = \sum_{d \in \mathcal{D}_j} q_{d,t} + \sum_{e \in \mathcal{E}_{j,t}} q_{e,t} - \sum_{s \in \mathcal{S}_j} q_{s,t}, \quad \forall j, t. \tag{28}$$

Considering the contribution of EVs and PVs as decision variables, the system optimal solution of Optimal Grid - DER coordination is obtained by the solution of the following SOCP optimization problem, referred to as **Full-opt**:

$$\textbf{Full-opt:} \quad (15) \quad \textit{subject to:} \quad (16)-(25), \; (27)-(28), (2)-(4), (7)-(13). \tag{29}$$

Let us now assume that the system-optimal DER schedules are $p^*_{s,t}$ and $q^*_{s,t}$ for PVs, and $p^*_{e,t}$ and $q^*_{e,t}$ for EVs. The DLMCs of the Full-opt solution at node j, time period t, reflecting the optimal DER schedules, are $\lambda^{P*}_{j,t}$ and $\lambda^{Q*}_{j,t}$. It is easy to show that if $\lambda^{P*}_{j,t}$ and $\lambda^{Q*}_{j,t}$ were the prices announced to each PV s and EV e, then the system-optimal PV and EV schedules would also be optimal for the PV-opt and EV-opt problems, respectively. To verify the above, consider the partial Lagrangian of Full-opt. It is obtained by appending the real and reactive power balance constraints (18)-(19) and substituting the net demand variables with (27)-(28). The terms that include the DER (PV/EV) variables in the partial Lagrangian are as follows:

$$\sum_{e,t} \left(\lambda^P_{j_e,t} p_{e,t} + \lambda^Q_{j_e,t} q_{e,t} \right) - \sum_{s,t} \left(\lambda^P_{j_s,t} p_{s,t} + \lambda^Q_{j_s,t} q_{s,t} \right),$$

where j_s refers to the node that PV s is installed, and j_e to the node that EV e is connected at time period t. The first sum coincides with the objective function of EV-opt, for $\lambda^P_{j_e,t} = \hat{\lambda}^P_t$ and $\lambda^Q_{j_e,t} = \hat{\lambda}^Q_t$, summed for all EVs. Similarly, the second sum coincides with the objective function of PV-opt summed for all PVs; the minus sign is obtained if we convert PV-opt to a minimization problem. Also, we note that PV constraints appear in both PV-opt and Full-opt, and that EV constraints appear in both EV-opt and Full-opt.

Let us consider the optimality conditions of Full-opt that involve DLMCs and DER variables (it is convenient to consider the partial Lagrangian representation), and the respective optimality conditions of PV-opt and EV-opt. It is rather straightforward to see that if we replace in PV-opt and EV-opt parameters $\hat{\lambda}^P_t$ and $\hat{\lambda}^Q_t$ with the DLMCs derived by the optimal solution of Full-opt, say $\lambda^{P*}_{j,t}$ and $\lambda^{Q*}_{j,t}$, with j referring to appropriate nodes j_s and j_e, respectively, then the optimality conditions of PV-opt and EV-opt will also be encountered in the optimality conditions of Full-opt that refer to PV and EV variables, respectively. Hence, an optimal solution of the Full-opt problem will also be optimal for the PV-opt and EV-opt problems if the prices announced to PVs and EVs reflect the respective DLMCs of the Full-opt solution.

Although only PVs and EVs are modeled in this paper as representative DER examples, other DERs can be treated similarly. The individual optimization problems suggest the following interpretation: Nodal marginal costs can be construed as prices that elicit a price-taking DER to adapt fully and self-schedule to its socially optimal real/reactive power profile. In other words, if we were able to determine these socially optimal spatiotemporal DLMCs and charge DERs on DLMC-based-prices, DERs would self-schedule in a manner that is optimal for the system as a whole.

We wish to note that DLMC-based pricing has attracted strong criticism that points to undesirable DLMC volatility. However, our numerical results provide overwhelming evidence that DER schedule adaptation to DLMC-based prices removes the volatility, which is indeed observed only when DERs schedule themselves in a manner that is not adaptive to the spatiotemporal DLMCs.

V. Hierarchical Decomposition

In this section, we present at a high-level the design of the proposed hierarchical decomposition approach. Having already introduced the DER and distribution network models, we show in this section how they can be used iteratively in the context of the proposed hierarchical decomposition.

Considering the two levels, DERs and Distribution networks, we call our approach "hierarchical", since at the higher level, Distribution Network Operators (DNOs) optimize their network operation conditional upon the DER self-dispatch, whereas at the lower level DERs self-dispatch optimizing their consumption/generation profile by adapting to tentative DLMC-based prices announced by DNOs. Notably, more levels could be introduced, considering the interplay at the sub-transmission network and even the transmission system. For the purposes of this paper, we present the two main levels of DERs and Distribution Networks, in order to convey the high-level idea of the proposed approach. The iterative algorith employed is sketched below.

Initialization: Obtain an initial guess of DLMCs, $\lambda^{P[0]}_t$, and $\lambda^{Q[0]}_t$ and announce them to the DERs. There are several ways to obtain such a guess. For instance, we can set the initial values equal to the LMPs and the opportunity cost for the provision of reactive power at the substation or we can solve Net-opt for an anticipated load forecast and/or anticipated DER dispatch.

Iteration $k+1$:

- **Step 1:** DERs (PVs and EVs) optimize their schedules for the announced DLMCs (solving PV-opt and EV-opt). Regularization terms are included in the PV-opt and EV-opt objective functions to deal with synchronization effects. Obtain: $p^{[k+1]}_{s,t}$, $q^{[k+1]}_{s,t}$, $\forall s \in \mathcal{S}$, and $p^{[k+1]}_{e,t}$, $q^{[k+1]}_{e,t}$, $\forall e \in \mathcal{E}$. Check for convergence of DER schedules. If not within tolerances, Go to Step 2.
- **Step 2:** For the optimal DER schedules obtained from Step 1, optimize the network operation, solving Net-opt

with net real (reactive) demand reflecting the updated DER schedules. Obtain new DLMCs, $\lambda_t^{P[k+1]}$, and $\lambda_t^{Q[k+1]}$. Go to next iteration (Step 1).

For clarity, we present the objective functions of PV-opt and EV-opt that include the added regularization terms, for iteration $k+1$ below:

$$\max_{p_{s,t},q_{s,t}} \sum_t \lambda_t^{P[k]} p_{s,t} + \sum_t \lambda_t^{Q[k]} q_{s,t} - \sigma \sum_t \left(p_{s,t} - p_{s,t}^{[k]}\right)^2 - \sigma \sum_t \left(q_{s,t} - q_{s,t}^{[k]}\right)^2, \quad (30)$$

$$\min_{p_{e,t},q_{e,t}} \sum_t \lambda_t^{P[k]} p_{e,t} + \sum_t \lambda_t^{Q[k]} q_{e,t} + \sigma \sum_t \left(p_{e,t} - p_{e,t}^{[k]}\right)^2 + \sigma \sum_t \left(q_{e,t} - q_{e,t}^{[k]}\right)^2. \quad (31)$$

Furthermore, we also show the updated aggregate net demand at iteration $k+1$ below:

$$p_{j,t} = \sum_{d \in \mathcal{D}_j} p_{d,t} + \sum_{e \in \mathcal{E}_{j,t}} p_{e,t}^{[k+1]} - \sum_{s \in \mathcal{S}_j} p_{s,t}^{[k+1]}, \quad \forall j,t, \quad (32)$$

$$q_{j,t} = \sum_{d \in \mathcal{D}_j} q_{d,t} + \sum_{e \in \mathcal{E}_{j,t}} q_{e,t}^{[k+1]} - \sum_{s \in \mathcal{S}_j} q_{s,t}^{[k+1]}, \quad \forall j,t. \quad (33)$$

The above iterative algorithm falls into the category of proximal algorithms. Although we do not provide a formal proof for convergence in this work, we sketch the key idea that is employed in the proof.

As discussed, the social optimum is obtained by the solution of the Full-opt problem presented in Section IV. The key is to observe that Full-opt falls into the setting provided in [30, Prop. 7.2.1]. The idea is to eliminate the network variables by expressing the optimal values as a function of the DER variables. Then, Full-opt can be solved using an iterative method that updates the DER variables based on (sub)gradients of the network part of Full-opt reflected by the DLMCs at Net-opt.

Lastly, we note that the proposed algorithm has several advantages. First, Step 1 scales to massive DER participation with accurate modeling of their costs/preferences, since each DER problem can be solved in parallel and very fast due to their size (they are small problems). Second, the regularization terms added in the DER problems avoid synchronization and if properly tuned — in an adaptive manner — they may speed up convergence — the idea is equivalent to scaling the regularization terms. Their magnitude also has an interesting interpretation that could be exploited in a practical setting: they represent the willingness of each DER to accept suboptimal solutions at each iteration. Third, the algorithm does not require the exchange of private DER information with the DNO, but only the real/reactive power profiles, which are also aggregated at each node — as we have seen Net-opt practically requires the aggregate net demand at each node and does not need to have DER-specific information. Fourth, the network problems fit nicely the operation of DNOs by solving AC OPF problems that do not require DER scheduling, since the DER dispatch is known. Hence, distribution utilities could use available tools/modules to solve Net-opt at Step 2. Fifth, the Net-opt problems are convex SOCP problems, and they do not depend on the number of DERs, since they only "see" aggregate demand. Hence, their solution depends mainly on the size of the network. Last but not least, a very important advantage of the proposed decomposition is that a feasible AC OPF solution for the Full-opt problem is available at each iteration. This is of paramount importance for practical implementations, since other decomposition approaches, e.g., dual decomposition or the popular Alternating Direction Method of Multipliers (ADMM) only provide a feasible solution when they converge.

VI. Numerical Illustration

We illustrate the applicability of the hierarchical decomposition on an actual 13.8 KV feeder of Holyoke Gas and Electric (HGE), a municipal distribution utility in MA, US. The feeder topology is shown in [6, Fig. 1], which also shows the commercial and residential load profiles as a percentage of the transformer nameplate capacity, the PV solar irradation factor, ρ_t, and the ambient temperature. Line and transformer data are listed in [6, Table I]. Lower voltage limits are set at 0.95 p.u. and upper voltage limits are set at 1.05 p.u. LMPs range from 25.59 to 53.48 ($/MWh). The opportunity cost for reactive power is assumed equal to 10% the value of the LMP.

Numerical experimentation focuses on two selected nodes, representing two 30-KVA transformers serving commercial and residential loads. To make results easier to follow while emphasizing the local effect of EVs and PVs on a distribution feeder, we consider different levels of EVs (0, 3, and 6 EVs) and of PVs (0, 30 KVA and 60 KVA) connected exclusively to these two nodes. At the commercial node, EVs are connected 9am–5pm and require charging 12 KWh. At the residential node, EVs are connected 7pm–7am and require charging 18 KWh. At the time of departure, EVs must be fully charged. EV battery capacity is 24 KWh, the maximum charging rate is 3.3 KW/h, and the charger capacity is 6.6 KVA. PVs are assumed to be 10-KVA rooftop solar. The regularization constant σ was set at 10,000. Also, to model initial conditions in the daily cycle reasonably, transformer temperatures were required to coincide at the beginning and at the end of the cycle, $t = 0$, and $t = 24$; a similar constraint was imposed on EV battery State of Charge. The optimization problems were solved on a Dell Intel Core i7-5500U @2.4 GHz with 8 GB RAM, using CPLEX 12.7, and solution times were up to 10 sec.

Before proceeding with the results of the decomposition, we should mention an important outcome of our enhanced AC OPF model. In our parallel work [5], [6], we have emphasized the importance of introducing transformer degradation in the short-run marginal costs, and we have provided analytical results that unbundle DLMCs into additive components, based on the cost of real and reactive power at the substation, real and reactive power marginal losses, voltage congestion,

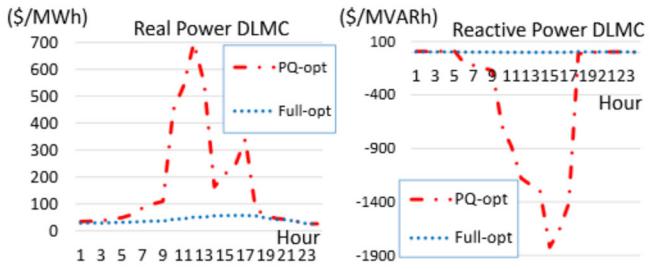

Fig. 2. Real power DLMCs (left) and reactive power DLMCs (right), under PQ-opt and Full-opt, for a 6-EV and 60-KVA PV penetration, at the commercial node.

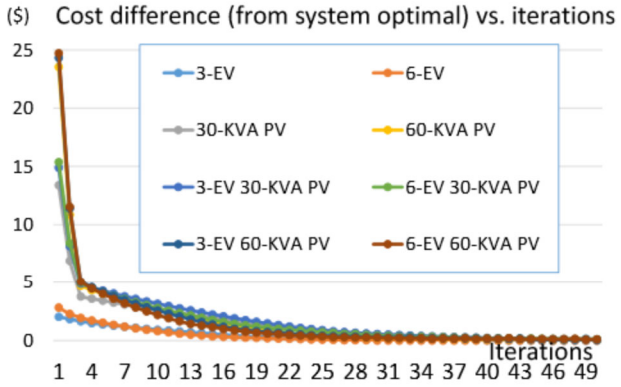

Fig. 3. Performance of the hierarchical decomposition approach for several DER penetrations; vertical axis shows the difference of the system cost from the system optimal at each iteration.

line (ampacity) congestion, and transformer degradation [5]. We have provided extensive numerical results [6] supporting the significant benefits of internalizing short-run marginal asset, primarily transformer, degradation, and that voltage and ampacity congestion DLMC components are insufficient in providing the price signal that supports the system optimal schedules. We have also demonstrated that apart from optimal short-run scheduling, our approach can harvest otherwise idle DER reactive power compensation capabilities, and increase distribution network DER hosting capacity mitigating investments in distribution infrastructure (see also our work on non wires solution [31], [32]). In this work, we only provide a simple example of how DLMCs convey the price signals to self-dispatching DERs.

In Fig. 2, we illustrate the DLMCs for real and reactive power for the case with 6 EVs and 60-KVA PV penetration at the commercial node for two scheduling options: (i) PQ-opt (as it is named in [6]), which refers to traditional line loss minimization, i.e., when DER schedules are obtained by minimizing the network losses, and (ii) Full-opt. The spikes observed at the PQ-opt values are due to the transformer component. Indeed such high DLMCs would be the result if we solved the AC OPF problem by minimizing only the cost for real and reactive power, since DERs would overutilize their inverter to reduce losses, without considering the local impact on the distribution transformer. In the context of the proposed decomposition, DER schedules will adapt to the price signals, e.g., EVs will shift their consumption, both EVs and PVs will adjust their reactive power profile, and as the solution approaches the system optimal, i.e., the Full-opt solution, DLMCs will become much smoother (see the Full-opt DLMCs).

In Fig. 3, we illustrate the convergence of the hierarchical decomposition for the various DER scenarios of EV/PV penetration. The vertical axis shows the difference in system cost (in $) from the system optimal solution at each iteration. The system optimal solution was obtained by solving Full-opt. The initialization was performed with the substation LMP and the opportunity cost for reactive power, and we observe that the cost at the first response of the DERs (first iteration) was up to 25$ higher compared to the system optimal for the 6 EV and 60-KVA penetration. The results illustrate that the algorithm practically converged — reached at or below 0.1 $ — in a few tens of iterations (we show up to the 50th iteration). These initial results are encouraging that by tuning the regularization terms (we kept them constant in this example), convergence may even be improved.

VII. Conclusions and Further Research

In this paper, we employ DLMCs as price signals that provide DERs with sufficient information to self-schedule in a manner interpretable as a minimization (maximization) of their individual cost (benefit). Indeed, DLMCs support optimal DER self-scheduling. A point of caution worth making is that DLMCs are not necessarily prices that, when charged, will render the distribution network whole in terms of allowing it to recover its variable and fixed costs. The difference of DLMCs during periods t and t' simply represents the change in the system (marginal) cost if a unit of power consumption is transferred from period t to period t'. For example, spatiotemporal DLMC-based prices may be set equal to a constant + the DLMC, as in a two-part tariff pricing approach. As long as the price differences across time and location equal the DLMC and the value of the constant is selected to provide adequate total revenue, the two-part tariff design will also support optimal DER self-scheduling.

We have also presented a hierarchical decomposition approach, which promises to enable Grid - DER coordination, allowing for massive DER participation, without relying on DER aggregators, while capturing with high fidelity the DER costs/preferences as well as the salient distribution network features. A preliminary numerical illustration has shown that this approach is quite promising reaching near-optimal solutions after some tens of iterations. Nevertheless, more numerical experimentation is required to evaluate the performance of the proposed decomposition, and compare it with alternative distributed schemes summarized in [33].

Lastly, we note that in our ongoing and future work, we aim at considering 3-phase representations of the distribution network and more DER types, such as micro generators, smart buildings with precooling/heating capable HVAC, smart appliances, storage. Furthermore, AC OPF

linearizations updated at each iteration combined with load flow solutions to refine the operating point around which DLMCs will be computed — seems a promising direction for a practical setup which we intend to pursue.

ACKNOWLEDGMENT

The authors would like to thank Holyoke Gas and Electric for providing actual feeder data for the numerical illustration.

REFERENCES

[1] S. Tierney, "Distributed energy resource valuation & integration," Electricity Advisory Committee, 2017.

[2] M. Caramanis, E. Ntakou, W. Hogan, A. Chakrabortty, and J. Schoene, "Co-optimization of power and reserves in dynamic T&D power markets with nondispatchable renewable generation and distributed energy resources," *Proc. IEEE*, vol. 104, no. 4, pp. 807–836, 2016.

[3] R. Tabors, G. Parker, P. Centolella, and M. Caramanis, "White paper on developing competitive electricity markets and pricing structures," Boston, MA, TCR Inc., Apr. 2016.

[4] E. Ntakou and M. Caramanis,"Price discovery in dynamic power markets with low-voltage distribution-network participants" *Proc. 2014 IEEE PES T&D Conf. & Exp.*, 15 - 17 April, Chicago, IL 2014.

[5] P. Andrianesis, and M. Caramanis, "Distribution network marginal costs - Part I: A novel AC OPF including transformer degradation," arXiv:1906.01570, 2019.

[6] P. Andrianesis, and M. Caramanis, "Distribution network marginal costs - Part II: Case study based numerical findings," arXiv:1906.01572, 2019.

[7] R. Li, Q. Wei, and S. Oren, "Distribution locational marginal pricing for optimal electric vehicle charging management," *IEEE Trans. Power Syst.*, vol. 29, no. 1, pp. 203–211, 2014.

[8] S. Huang, Q. Wu, S. S. Oren, R. Li, and Z. Liu, "Distribution locational marginal pricing through quadratic programming for congestion management in distribution networks," *IEEE Trans. Power Syst.*, vol. 30, no. 4, pp. 2170–2178, 2015.

[9] L. Bai, J. Wang, C. Wang, C. Chen, and F. Li, "Distribution Locational Marginal Pricing (DLMP) for congestion management and voltage support," *IEEE Trans. Power Syst.*, vol. 33, no. 4, pp. 4061–4073, 2018.

[10] M. C. Caramanis, R. R. Bohn, and F. C. Schweppe, "Optimal spot pricing: Practice and theory," *IEEE Trans. Power App. Syst.*, vol. PAS-101, no. 9, pp. 3234–3245, 1982.

[11] F. C. Schweppe, M. C. Caramanis, R. D. Tabors, and R. E. Bohn, *Spot pricing of electricity*, Kluwer Academic Publishers, 1988.

[12] M. E. Baran, and F. F. Wu, "Optimal capacitor placement on radial distribution systems," *IEEE Trans. Power Del.*, vol.4, no.1, pp. 725–734, 1989.

[13] M. Farivar, and S. Low, "Branch-flow model: Relaxations and convexification - Part I," *IEEE Trans. Power Syst.*, vol. 28, no. 3, pp. 2554–2564, 2013.

[14] A. Papavasiliou, "Analysis of distribution locational marginal prices," *IEEE Trans. Smart Grid*, vol. 9, no. 5, pp. 4872–4882, 2018.

[15] "The EV Project, 2013, What Clustering Effects have been seen by The EV Project?," https://avt.inl.gov/sites/default/files/pdf/EVProj/126876-663065.clustering.pdf.

[16] Smart Electric Power Alliance and Black & Veatch, "Planning the Distributed Energy Future, Volume II: A case study of utility integrated DER planning from Sacramento Municipal Utility District," May 2017.

[17] Q. Gong, S. Midlam-Mohler, V. Marano, and G. Rizzoni, "Study of PEV charging on residential distribution transformer life," *IEEE Trans. Smart Grid*, vol. 3, no. 1, pp. 404–412, 2012.

[18] A. D. Hilshey, P. D. H. Hines, P. Rezaei, and J. R. Dowds, "Estimating the impact of electric vehicle smart charging on distribution transformer aging," *IEEE Trans. Smart Grid*, vol. 4, no. 2, pp. 905–913, 2013.

[19] K. Qian, C. Zhou, and Y. Yuan, "Impacts of high penetration level of fully electric vehicles charging loads on the thermal ageing of power transformers," *Int. J. El. Power En. Syst.*, vol. 65, pp. 102–112, 2015.

[20] Y. O. Assolami, and W. G. Morsi, "Impact of second-generation plug-in battery electric vehicles on the aging of distribution xtransformers considering TOU prices," *IEEE Trans. Sustainable Energy*, vol. 6, no. 4, pp. 1606–1614, 2015.

[21] M. S. ElNozahy, and M. M. A. Salama, "A comprehensive study of the impacts of PHEVs on residential distribution networks," *IEEE Trans. Sustainable Energy*, vol. 5, no. 1, pp. 332–342, 2014.

[22] M. K. Gray, and W. G. Morsi, "On the role of prosumers owning rooftop solar photovoltaic in reducing the impact on transformer's aging due to plug-in electric vehicles charging," *Electric Power Syst. Res.*, vol. 143, pp. 563-572, 2017.

[23] IEEE Guide for Loading Mineral-Oil-Immersed Transformers, IEEE Standard C57.91, 2011.

[24] BS IEC 60076-7:2018, Power Transformers, Part 7: Loading guide for mineral-oil-immersed power transformers, 2018.

[25] S. Y. Abdelouadoud, R. Girard, F. P Neirac, and T. Guiot, "Optimal power flow of a distribution system based on increasingly tight cutting planes added to a second order cone relaxation," *Int. J. Electr. Power Energy Syst.*, vol. 69, pp. 9–17, 2015.

[26] S. Huang, Q. Wei, J. Wang, and H. Zhao, "A sufficient condition on convex relaxation of AC optimal power flow in distribution networks," *IEEE Trans. Power Syst.*, vol. 32, no. 2, pp. 1359–1368, 2017.

[27] W. Wei, J. Wang, N. Li, and S. Mei, "Optimal power flow of radial networks and its variations: A sequential convex optimization approach," *IEEE Trans. Smart Grid*, vol. 8, no. 6, pp. 2974–2987, 2017.

[28] M. Nick, R. Cherkaoui, J.-Y. Le Boudec, and M. Paolone, "An exact convex formulation of the optimal power flow in radial distribution networks including transverse components," *IEEE Trans. Autom. Control*, vol. 63, no. 3, pp. 682–697, 2018.

[29] Z. Yuan, M. R. Hesamzadeh, and D. R. Biggar, "Distribution locational marginal pricing by convexified ACOPF and hierarchical dispatch," *IEEE Trans. Smart Grid*, vol. 9, no. 4, pp. 3133–3142, 2018.

[30] D. P. Bertsekas, 2016. Nonlinear Programming. Third Edition. Athena Scientific, Belmont, MA.

[31] R. Tabors, P. Andrianesis, M. Caramanis, and R. Masiello, "The value of distributed energy resources to the grid: Introduction to the concepts of marginal cost of capacity and locational marginal value," in Proc. 52nd HICCS, 2019, Maui, HI, 8-11 Jan. 2019

[32] P. Andrianesis, M. Caramanis, R. Masiello, R. Tabors, and S. Bahramirad, "Locational marginal value of distributed energy resources as non wires alternatives," *IEEE Trans. Smart Grid*, accepted, 2019.

[33] D. K. Molzahn, F. Dörfler, H. Sandberg, S. H. Low, S. Chakrabarti, R. Baldick, and J. Lavaei, "A survey of distributed optimization and control algorithms for electric power systems," *IEEE Trans. Smart Grid*, vol. 8, no. 6, pp. 2941–2962, 2017.